Rotational and translational diffusion of fluorocarbon tracer spheres in semidilute xanthan solutions

Gijsberta H. Koenderink,[1] Stefano Sacanna,[2] Dirk G. A. L. Aarts,[2] and A. P. Philipse[2,*]

[1]*Physics of Complex Systems, Vrije Universiteit, De Boelelaan 1081, 1081 HV Amsterdam, The Netherlands*

[2]*Van't Hoff Laboratory for Physical and Colloid Chemistry, Debye Institute, Utrecht University, Padualaan 8, 3584 CH Utrecht, The Netherlands*

We report an experimental study of rotational and translational diffusion and sedimentation of colloidal tracer spheres in semidilute solutions of the nonadsorbing semiflexible polymer xanthan. The tracers are optically anisotropic, permitting depolarized dynamic light scattering measurements without interference from the polymer background. The xanthan solutions behave rheologically like model semidilute polymeric solutions with long-lived entanglements. On the time scale of tracer motion the xanthan solutions are predominantly elastic. The generalized Stokes-Einstein relation describing the polymer solution as a continuous viscous fluid therefore severely overestimates the tracer hindrance. Instead, effective medium theory, describing the polymer solution as a homogeneous Brinkman fluid with a hydrodynamic screening length equal to the concentration-dependent static correlation length, is in excellent agreement with the tracer sedimentation and rotational diffusion coefficients. Rotational diffusion, however, is at the same time in good agreement with a simple model of a rotating sphere in a concentric spherical depletion cavity. Translational diffusion is faster than predicted for a Brinkman fluid, likely due to polymer depletion.

I. INTRODUCTION

The retardation of particle transport in entangled polymer solutions and gels plays a key role in a wide range of technological and biological processes. Accordingly, the topic has attracted much experimental and theoretical attention. Most work has focused on the *translational* diffusion of tracers, commonly measured with dynamic light scattering [1–7] (DLS). Though various theoretical models for translational diffusion of tracers in polymer matrices have been proposed [8–10], the mechanisms of retardation are still incompletely understood. In contrast, experimental [11] and theoretical work [12,13] on the *rotational* diffusion of colloidal spherical tracers in polymer solutions is scarce. Rotational diffusion of spherical tracers is a local dynamic process that is less sensitive to sterical hindrance than translational diffusion. Differences between the translational and rotational viscous drag on a spherical tracer in a polymer matrix could thus be used to probe the solution microstructure [13].

In this paper we present measurements of the rotational and translational diffusion coefficients of spherical tracer colloids in semidilute solutions of the semiflexible polyelectrolyte xanthan. The tracers, which are made of a fluorocarbon polymer, are optically anisotropic, permitting depolarized dynamic light scattering (DDLS) measurements [11,14,15]. DDLS yields rotational and translational diffusion coefficients of the tracer in a single experiment without the complications inherent to DLS of contributions from the polymer background. The xanthan polymer is a microbial polysaccharide secreted by the plant pathogenic bacterium

Xanthomonas. Xanthan has been the subject of many physicochemical studies, partly because of its widespread use as a thickener and stabilizer of water-based industrial and consumer products [16]. In aqueous electrolyte solutions, xanthan molecules form double helices with a persistence length of 120 nm [17–20]. It has been established that xanthan solutions in $0.1M$ aqueous NaCl are excellent model systems for semiflexible wormlike polymers in a good solvent. At concentrations c_p above the overlap concentration c_p^*, and for sufficiently large molecular weight, the interactions between the polymer chains are dominated by topological entanglements. In this work we will focus on this entangled regime, using a large molecular weight xanthan sample (4 $\times 10^6$ g/mol) with a contour length of 2 μm, i.e., eight Kuhn statistical segments per chain, at concentrations c_p up to $30c_p^*$. The xanthan solutions are optically transparent and isotropic and therefore do not interfere with the DDLS measurements. The experiments are carried out under conditions where double-layer interactions between the negatively charged polymer and tracer particles are screened. The investigations are restricted to tracer and polymer concentrations where phase separation is absent. At larger colloid and polymer concentrations the mixtures phase separate due to depletion-induced attractions between the tracers [21].

One aim of this work is to compare the friction factors for rotational and translational diffusion of the spherical tracers in entangled xanthan solutions. In the absence of polymer, the friction factors are the Stokes drag coefficients f_0^t and f_0^r [22]. The translational drag f_0^t is proportional to the tracer particle radius a_T,

$$f_0^t = 6\pi\eta_0 a_T, \tag{1}$$

while the rotational drag f_0^r is proportional to the particle volume,

---

*Author to whom correspondence should be addressed. Email address: fccoffice@chem.uu.nl

$$f_0^r = 8\pi\eta_0 a_T^3, \qquad (2)$$

where η_0 is the solvent viscosity. We investigate how the rotational and translational drag coefficients are affected by hydrodynamic interactions of the tracer particle with the surrounding polymer solution. Apart from tracer diffusion, we also measure the friction on a sedimenting tracer. In the absence of polymer, sedimentation is governed by the same translational drag coefficient f_0^t as the translational diffusion coefficient. In a polymer solution, however, the friction factors for sedimentation and translational diffusion are often different [23–25]. The reason is that hydrodynamic and direct interactions of the tracer particle with the polymers generally leads to a frequency dependence of the friction. Since sedimentation and translational diffusion take place on entirely different length and time scales, the drag on a tracer in a polymer solution may differ for the two transport processes.

An interpretation of the diffusion and sedimentation results requires a knowledge of the dynamics of the entangled xanthan solutions, since the dynamics of the tracer particles are coupled to the polymer dynamics. Accordingly, we extensively characterize the xanthan solution dynamics in terms of the rheological response to steady and oscillatory shear. It is shown that the xanthan solutions behave rheologically like model semidilute polymeric solutions with long-lived entanglements. Since the lifetime of the transient entanglements as determined from oscillatory shear measurements is longer than the rotational and translational diffusion times of the tracers, the measured tracer diffusion coefficients are short-time quantities. On the time scale of tracer diffusion the xanthan background is essentially static, so the tracer mobility is affected only by hydrodynamic interactions and not by the tortuosity of the polymer network. Accordingly, the data are analyzed in terms of theoretical models for hydrodynamic hindrance of particle transport. Additionally, the diffusion and sedimentation coefficients are compared with the inverse low-shear viscosity of the xanthan solutions, to test whether the Stokes relations in Eqs. (1) and (2) can be generalized to tracer diffusion in polymer solutions.

II. EXPERIMENTAL METHODS

A. Xanthan solutions

Xanthan is a polymer built of five-sugar repeating units consisting of a dimeric β-D-glucose backbone segment identical to that of cellulose, with a charged three-sugar side chain attached to every second backbone glucose. The degrees of pyruvyl and acetyl substitution $\mathcal{S}_{ace}$ and $\mathcal{S}_{pyr}$ of the side chains vary with the fermentation conditions. We used SKW Biosystems xanthan (weight-averaged molecular weight $M = 4 \times 10^6$ g/mol [26]) with $\mathcal{S}_{ace} \approx 0.8$ and $\mathcal{S}_{pyr} \approx 0.5$ [27]. A xanthan stock solution was prepared by dissolving xanthan powder in water containing $0.1M$ NaCl, to screen double-layer repulsions, and 2 mM of the antimicrobial agent sodium azide (NaN$_3$). The solution was heated under continuous magnetic stirring until the solution temperature reached 85 °C, at which point heating was stopped and the solution was slowly cooled and stirred for 15 h. Heat

treatment of xanthan solutions removes aggregates [26,28,29]. Heating was done in the presence of $0.1M$ NaCl to make sure that the conformation of xanthan is an ordered double-helix. At NaCl concentrations below 5 mM the xanthan conformation is a disordered flexible coil due to mutual repulsions between the charged side chains [26]. The maximum temperature is chosen below the characteristic melting temperature T_m (~ 100 °C) where the xanthan double-helix is disrupted [26,30–32]. Cooling below T_m is known to result in the formation of a weakly cross-linked network of partially double-stranded xanthan [33].

The double-helices have a hydrodynamic diameter of 2.2 nm in aqueous solution and a weight-averaged contour length $L_c = 2$ μm (the molar mass M_L per unit contour length [28,31,34,35] is 1940 g mol^{-1} nm^{-1}). The persistence length of double-helical xanthan as deduced from light scattering, viscosity and sedimentation measurements was reported to be in the range $q = 100$–150 nm [28,31,34,35], with one report [36] suggesting a much smaller value $q = 65$ nm. The number of Kuhn statistical segments $N_k = L_c/2q$ per chain, using the consensus value $q = 120$ nm, equals 8, so the xanthan chains are semiflexible. The radius of gyration R_g is 264 nm according to the Benoît-Doty formula [37] for wormlike polymers. The Benoît-Doty expression assumes that the chains are stiff enough ($L_c/q \ll q/D$) for excluded volume effects to be negligibly small, which is true for xanthan [38]. The overlap concentration c_p^* $= 3M/(N_{av}4\pi R_g^3)$ is about 0.008 wt %. The maximum concentration of 0.219 wt % used is far below the onset of nematic ordering (>0.5 wt %). Polymer concentrations c_p in units of weight percent were converted to volume fractions ϕ using the known specific volume (0.62 g/cm^3) of xanthan in $0.1M$ aqueous NaCl [31,39,40]. The maximum volume fraction used is 0.0014.

B. Rheological characterization of xanthan solutions

Rheological experiments were performed with a controlled-stress Paar Physica MCR 300 rheometer, using a cone-plate geometry with a diameter of 50 mm, a cone angle of 1°, and a truncation of 51 μm. Steady-shear experiments were carried out using shear rates $\dot{\gamma}$ from 10^{-3} to 50 s^{-1}. There was no hysteresis between increasing and decreasing shear rate ramps. The zero-shear-limiting viscosity η_L, normalized by the solvent viscosity ($\eta_0 = 0.866$ mPa s), was determined by extrapolation of the flow curves to $\dot{\gamma} = 0$. Oscillatory shear experiments were done at frequencies ω between 10^{-3} and 100 rad/s, using a constant strain γ between 0.05 and 0.5. The applied strain varied with c_p, being chosen small enough to remain in the linear viscoelastic regime and large enough to give a torque of at least 10 nN m. The observable is the complex shear modulus $G^* = G' + iG''$, which has an elastic component, the storage modulus G', and a dissipative viscous component, the loss modulus G''.

C. Depolarized dynamic light scattering (DDLS) measurements

Optically anisotropic tracer spheres were fluorocarbon PFA particles prepared by dispersion copolymerization of

tetrafluoroethylene with perfluoromethylvinylether in water, in the presence of an anionic perfluorinated surfactant [41]. The particles were kindly donated by Ausimont S.p.A. (Milano, Italy). The particles bear a negative surface charge due to adsorbed fluorinated surfactant and to carboxyl end groups of the polymer chains generated by the decomposition of the initiator [41]. Their internal structure is believed to be an irregular packing of crystallites formed by folded ribbons of polymer chains with a chain folding length of the order of 50 nm, dispersed in an amorphous matrix. The number of crystallites N is too small ($N \approx 10$–30) to result in a complete randomization of the direction of the polarizability axes. The effective optical anisotropy of the polycrystalline particles is only reduced by a factor of order $N^{1/2}$ compared to the anisotropy of a monocrystalline polytetrafluoroethylene particle of the same size [41]. The particles have a mass density ρ_p of 2.14 g/ml [42]. In water, the PFA particles are stable up to NaCl concentrations of at least 100 mM. The hydrodynamic radius in water as derived from the translational diffusion coefficient D_0^t is $a_{\text{DLS}} = 93$ nm according to DLS and $a_{\text{DDLS},t} = 92$ nm according to DDLS. The hydrodynamic radius $a_{\text{DDLS},r}$ in water from the rotational diffusion coefficient D_0^r is 95 nm.

The short-time translational and rotational diffusion coefficients, D_s^t and D_s^r, of the PFA tracer spheres (volume fraction 0.002) in xanthan solutions were measured with depolarized dynamic light scattering. Tracer concentrations were low enough to prevent multiple scattering, preclude tracer-tracer interactions, and avoid sphere clustering due to depletion attraction [21]. DDLS measurements were performed at 25 °C, using light from a polarized argon laser (Spectra Physics model 2000) with a wavelength $\lambda_0 = 514.5$ nm and a power of 400 mW. The incident beam was linearly polarized in the vertical direction using a Glan-Taylor polarizer. The horizontal (I_{VH}) and vertical (I_{VV}) polarized scattered intensities were selected with a Glan-Thompson polarizer placed in front of the photomultiplier. Intensity autocorrelation functions (IACFs) were accumulated with a 128 channel correlator (Malvern 7032 CE) at seven angles θ between 30° and 120°, corresponding to wave vectors $k = 4\pi n_s \sin(\theta/2)/\lambda_0$ in the range $(0.84$–$2.8) \times 10^7$ m^{-1}. The normalized IACFs were fitted to the second order cumulant expression $g_1(k,t) = A + B \exp(\Gamma t + C t^2)$, where Γ represents the decay rate and C accounts for polydispersity in particle size and optical properties. A plot of $\Gamma(k) = 12 D_s^r + 2 D_s^t k^2$ versus k^2 has a slope $2 D_s^t$ and an intercept $12 D_s^r$. DDLS data for xanthan concentrations $c_p > 0.148$ wt % were excluded, since Γ was no longer linear in k^2, most likely due to the occurrence of depletion-induced phase separation [21].

D. Sedimentation velocity measurements

The sedimentation coefficients s of PFA tracer spheres (volume fraction 0.009) in xanthan solutions with concentrations $c_p \leqslant 0.1$ wt % were measured under gravity by monitoring the traveling distance h of the interface separating the lower colloid-containing xanthan phase and the upper clear xanthan supernatant. Mixtures were homogenized by vigorous shaking, defining time $t=0$ as the moment when shaking

was stopped, and placed on a heavy marble table, to prevent vibrations, in a temperature controlled room (24 °C). The sedimentation coefficient s was obtained as the slope dh/dt, divided by the gravitational constant, $g = 9.80665$ m/s^2. Sedimentation coefficients were normalized by the value s_0 measured in absence of xanthan. The experimental s_0 value of $14089 S$ (corresponding to an apparent sphere radius of 69 nm) deviates significantly from the theoretical value, $s_0 = 25289$ S, following from the Stokes velocity

$$s_0 = \frac{2 a_T^2 \Delta \rho}{9 \eta_0}, \qquad (3)$$

using a density difference between particle and solvent of $\Delta \rho = 1140$ kg/m^3. This discrepancy may be partly due to repulsive tracer-tracer interactions. Other factors may also be important, such as a sedimentation potential, generated by sedimenting charged particles [43]. Here we also note the reduction of the effective mass of sedimenting charged colloids, even at a high ionic strength, observed by Piazza *et al.* [44]. (The possibility of an electric field counteracting gravity has been demonstrated by simulations [45] and is also confirmed by recent theory [46].) Normalizing s by s_0 removes the effect of any tracer-tracer interactions, provided that these interactions are not modified in the presence of polymer.

III. RESULTS

A. Steady-shear rheology of xanthan solutions

Figure 1(A) shows representative flow curves for xanthan solutions with concentrations c_p between 0.038 and 0.219 wt %. All solutions were shear thinning above a critical shear rate $\dot{\gamma}_c$ that steadily decreased from 65 to 0.34 s^{-1} with increasing c_p, indicating a progressive slowing-down of the polymer dynamics. For shear rates $\dot{\gamma} > \dot{\gamma}_c$ the flow curves exhibit a power-law behavior $\eta \propto \dot{\gamma}^{-m}$, typical of semidilute polymeric solutions, with a shear-thinning index m that increases monotonically from 0 at $c_p = 0$ to 0.7 at $c_p = 0.219$ wt % [Fig. 1(B)]. The reduced low-shear-limiting viscosity η_L/η_0 in the Newtonian region at vanishing shear rate ($\dot{\gamma} \to 0$) is plotted in Fig. 2(A) as a function of the xanthan concentration c_p. In the dilute regime, below the overlap concentration c_p^*, the viscosity of a polymeric solution follows [47]:

$$\eta_{sp} = (\eta_L/\eta_0 - 1)/c_p = [\eta] + k'[\eta]^2 c_p, \qquad (4)$$

with specific viscosity η_{sp}, intrinsic viscosity $[\eta]$ and Huggins coefficient k'. The specific viscosity is linear in c_p up to $c_p \approx 0.035$ wt %, with intercept $[\eta] = 3012 \pm 2546$ ml/g and Huggins coefficient $k' = 4 \pm 1$ [dotted line in Fig. 2(B)]. Capron *et al.* [26,48] reported $[\eta] = 7150$ ml/g and $k' = 0.6$ for xanthan supplied by the same company (SKW-Biosystems). However, these authors dissolved xanthan in water in the absence of salt at 4 °C, a procedure that presumably gives a different solution microstructure with more aggregates than the procedure used here. For xanthan with a molecular
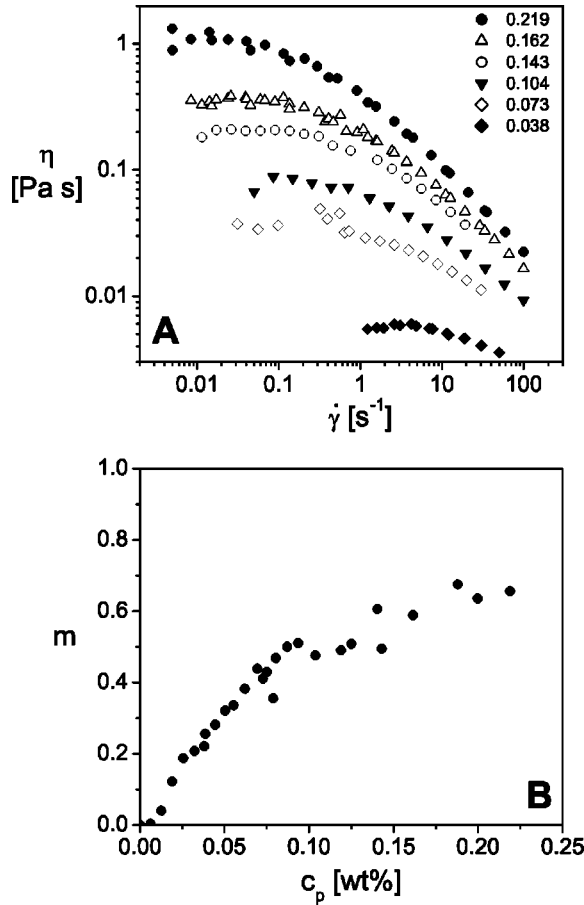
FIG. 1. Steady-shear measurements on aqueous xanthan solutions containing 0.1M NaCl and 2 mM NaN$_3$. (A) Apparent viscosity $\eta(\dot{\gamma})$ vs shear rate $\dot{\gamma}$ for various xanthan concentrations c_p, as indicated. (B) Shear-thinning index $m(c_p)$, quantifying the asymptotic power-law shear-thinning behavior, $\eta \propto \dot{\gamma}^{-m}$.

weight of 4×10^6 g/mol one expects from the experimentally known [18,31] $[\eta]$-M relationship, $[\eta] \cong 5.3 \times 10^4$ ml/g, while k' is known [49] to lie in the range of 0.30–0.40 for polymers in good solvents. For concentrations $c_p / c_p^* \cong 1 - 10$ the overlap of individual polymer coils is the dominant type of intermolecular interaction and the viscosity is described by the Martin equation

$$\eta_{sp} = [\eta] \exp\{k[\eta]c_p\}, \tag{5}$$

where k in practice often equals k'. Fitting Eq. (5) to the data in the range $c_p = 0.035 - 0.08$ wt % [solid line in Fig. 2(C)] gives $[\eta] = 6247 \pm 1079$ ml/g and $k = 0.46 \pm 0.04$. Above $c_p = 10c_p^*$ the dominant intermolecular interaction is the topological constraint that polymers cannot cross each other [50,51]. Various scaling theories for long entangled chains predict $\eta_L / \eta_0 \propto c_p^\kappa$ with $\kappa = 3.5$ [52]. Indeed η_L / η_0 exhibits a power-law behavior for $c_p \gtrsim 11c_p^*$, with $\kappa = 3.2 \pm 0.1$ [inset of Fig. 2(A)], in agreement with previous experimental findings [18,29,53,54] ($\kappa = 3-3.7$). Larger exponents of 5–8 have occasionally been found for large molecular weight xanthan [18,33], which was ascribed to transient cross-
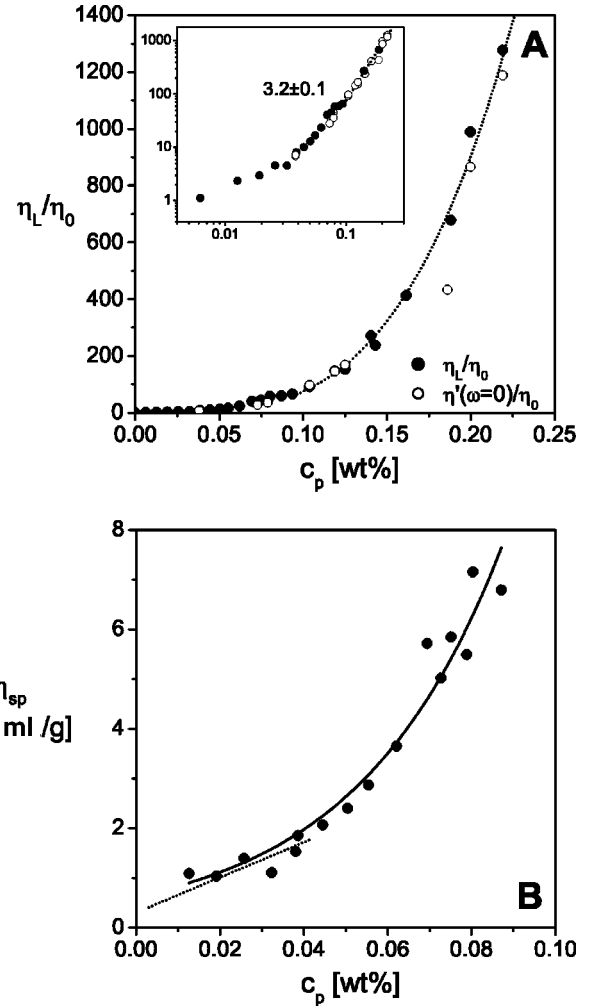

FIG. 2. (A) Reduced low-shear viscosity η_L / η_0 of aqueous xanthan solutions as a function of the xanthan concentration c_p. Open circles represent reduced low-frequency-limiting dynamic viscosity $\eta'(\omega=0)/\eta_0$. Dotted lines represent asymptotic power-law fits $\eta_L / \eta_0 \propto c_p^{3.2\pm0.1}$ for $c_p \gtrsim 0.1$ wt %. The inset graph is a log-log representation of the same data. (B) Specific viscosity η_{sp} vs c_p, with fits to Eq. (4) in the regime $c_p < c_p^*$ (dotted line) and to Eq. (5) in the range $c_p = (1-10)c_p^*$ (solid line).

linking due to hydrogen bonding or hydrophobic interactions. Since in this work the scaling of η_L / η_0 with c_p is entirely consistent with purely topological entanglements between chains, we believe that cross-linking is absent.

B. Oscillatory shear rheology of xanthan solutions

Figure 3(A) shows the frequency dependencies of the linear viscoelastic storage and loss moduli, G' and G'', of xanthan solutions with $c_p = 0.073$ and 0.219 wt %. The moduli increase appreciably as c_p is raised. The xanthan solutions are viscoelastic, being predominantly viscous at low frequencies ($G'' > G'$) and predominantly elastic at high frequencies ($G' > G''$). At low frequencies the loss moduli approach the scaling $G'' \propto \omega$ characteristic of Newtonian polymeric solutions without significant entanglements [55]. The frequency ω_c where G' and G'' cross decreases from 63 rad/s at c_p
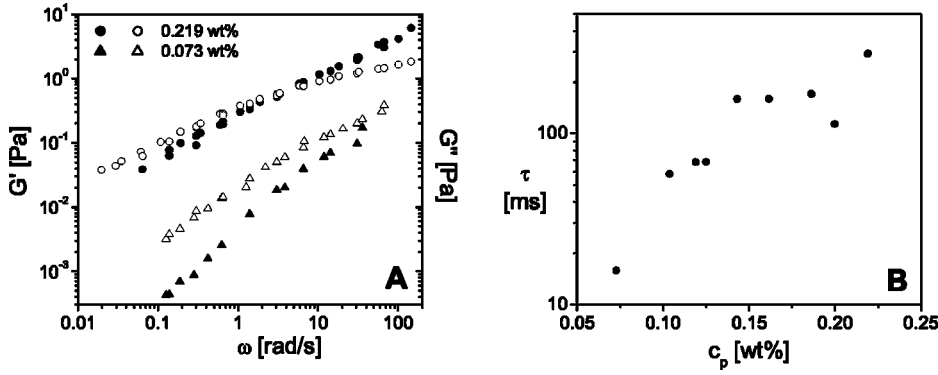
FIG. 3. (A) Storage modulus G' (closed symbols) and loss modulus G'' (open symbols) of aqueous xanthan solutions with $c_p = 0.073$ and 0.219 wt %, as a function of the radial frequency ω. (B) Crossover time $\tau_c = 1/\omega_c$, where $G'' = G'$.

$=0.073$ wt % to 3 rad/s at $c_p = 0.219$ wt %. The crossover frequency ω_c corresponds to a characteristic relaxation time $\tau_c = 1/\omega_c$ associated with the lifetime of the entanglements. For times $t < \tau_c$ the polymer solution behaves as a transient gel with principally elastic response, while for long times $t > \tau_c$ the entanglements relax on a time scale smaller than the time scale of oscillation and the polymer solution is predominantly viscous. As shown in Fig. 3(B), τ_c increases from 16 to 300 ms on going from 0.073 to 0.219 wt % xanthan.

Interestingly, the frequency dependence of the absolute magnitude of the linear viscoelastic complex viscosity,

$$|\eta^*| = \sqrt{(G')^2 + (G'')^2}/\omega, \qquad (6)$$

is virtually identical to the shear rate dependence of the steady shear viscosity $\eta(\dot{\gamma})$, in accordance with the empirical Cox-Merz rule [56] (see Fig. 4). Apparently the response of the solutions to steady shear is governed by the same relaxation processes as the response to oscillatory shear. Previous rheological studies of xanthan solutions have likewise found the Cox-Merz rule to be fairly accurate [57], except in cases where the chains associated by non-covalent interactions to form weak gel-like networks [54]. Figure 4 therefore supports our belief that the xanthan chains are not cross-linked but only temporarily congested by topological entanglements.
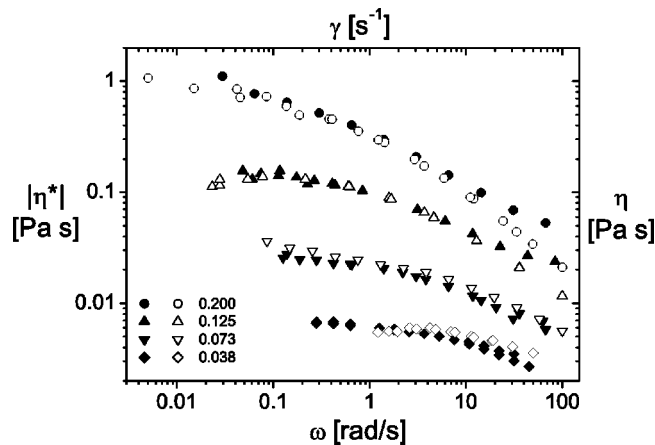

FIG. 4. Experimental test of the empirical Cox-Merz rule, stating that the steady-shear viscosity $\eta(\dot{\gamma})$ (open symbols) is identical to the complex viscosity $|\eta^*(\omega)|$ (closed symbols), for xanthan solutions with various concentrations c_p as indicated.

C. Tracer diffusion and sedimentation in xanthan solutions

Figure 5 shows the reduced short-time rotational and translational diffusion coefficients, H_s^r and H_s^t, of PFA tracer spheres in xanthan solutions as a function of the xanthan concentration c_p. The absence of a strong decline of the diffusion coefficients on addition of xanthan indicates that xanthan does not adsorb onto the PFA tracers. The rotational diffusion coefficient is particularly sensitive to any adsorption effects due to the strong dependence of the friction factor on the tracer radius a_T [Eq. (2)]. We note in addition that all intensity autocorrelation functions were single exponential and decayed to zero.

Rotational and translational tracer diffusion are slowed to the same extent by the polymer matrix, reaching circa 50% of their infinite dilution values at the highest xanthan concentration used (0.15 wt %). The c_p dependencies are fairly
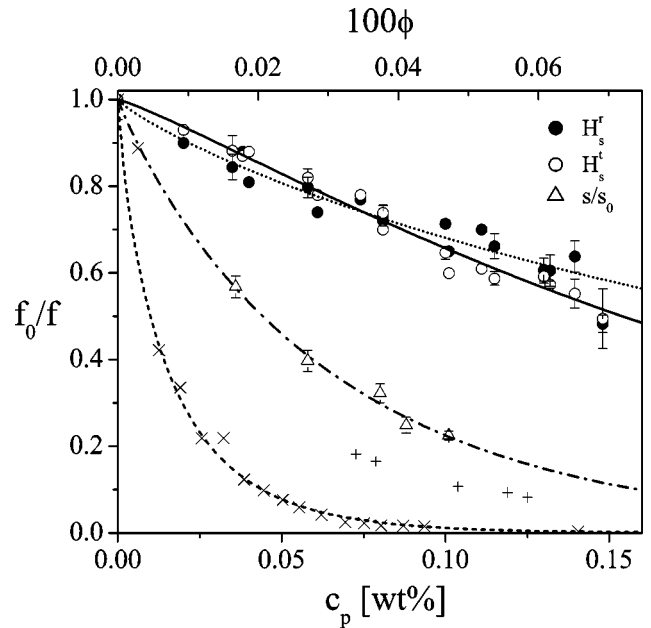

FIG. 5. Reduced rotational and translational diffusion coefficients, H_s^r and H_s^t, and reduced sedimentation coefficient s/s_0 of PFA tracer spheres in xanthan solutions as a function of the xanthan concentration c_p. Crosses represent the inverse reduced low-shear viscosity η_0/η_L. Plus signs represent the inverse reduced dynamic viscosity, η_0/η_{67}, measured at $\omega = 67$ rad/s. Lines are fits to the stretched exponential, Eq. (7). The upper X axis shows the volume percentage of xanthan, calculated from c_p as explained in Sec. II A.

well described by the stretched exponential form (solid lines)

$$f_0^{(a)}/f^{(a)}(c_p) = \exp(-\alpha c_p^{\nu}), \qquad (7)$$

with $f_0^{(a)}$ and $f^{(a)}$ the friction coefficients in the absence and presence of polymer, respectively ($a \in [r,t]$). The stretched exponential form generally correlates well with experimental data on tracer diffusion [3,58–60] and sedimentation [23–25,61–63], though consensus on the magnitude and physical interpretation of the fitting parameters α and ν is lacking. The exponent ν, for instance, typically varies between 0.5 and 1. The match of Eq. (7) with data for many different systems is not surprising given the flexibility of this fitting function. For the rotational drag the best fit values are $\alpha = 3 \pm 1$ and $\nu = 0.85 \pm 0.07$, while for the translational drag the best fit values are $\alpha = 6 \pm 1$ and $\nu = 1.16 \pm 0.04$. For comparison we mention that Jamieson *et al.* [53] found an exponent $\nu = 0.5$ for DLS data on translational diffusion of latex tracer spheres ($a_T = 100$ nm) in xanthan solutions ($M = 2.2 \times 10^6$ g/mol). In contrast to this work, however, their results were obtained in the absence of NaCl, where the conformation of xanthan is disordered and more flexible than in the presence of 0.1*M* NaCl.

Figure 5 also displays the c_p dependence of the normalized sedimentation coefficient s/s_0 of the PFA tracer spheres in xanthan solutions. Interestingly, the friction coefficient $f(c_p)$ is considerably larger for tracer sedimentation than for tracer diffusion. At $c_p = 0.1$ wt %, for instance, $s/s_0 = 0.22$ while $H_s^r \approx H_s^t \approx 0.65$. The c_p dependence of the reduced drag $s/s_0 = f_0/f$ is again well described by the stretched exponential expression [Eq. (7)], with best fit values $\alpha = 13 \pm 1$ and $\nu = 0.94 \pm 0.06$.

The Stokes friction factors of tracer spheres in pure solvent are proportional to the solvent viscosity η_0, as specified in Eqs. (1) and (2). A much investigated issue [16,24,60,64,65] is whether the Stokes relations can be generalized for tracers in polymer solutions, by replacing η_0 by the low-shear viscosity η_L:

$$f_0^{(a)}/f^{(a)}(c_p) = \eta_0/\eta_L(c_p). \qquad (8)$$

The crosses in Fig. 5 represent the inverse low-shear viscosity η_0/η_L of the xanthan solutions. Clearly, the macroscopic solution viscosity η_L/η_0 grossly overestimates the effective viscosity $\eta_{\text{eff}} = f/f_0$ experienced by the PFA tracers. The deviation grows continuously with increasing c_p to a factor $H_s^r \eta_L/\eta_0 \approx H_s^t \eta_L/\eta_0$ of 160 at $c_p = 0.15$ wt % for rotational and translational diffusion, and a factor $s \eta_L/s_0 \eta_0$ of 22 at $c_p = 0.1$ wt % for sedimentation. Similarly large deviations were found by Jamieson *et al.* [53] for the translational diffusion coefficient of polystyrene spheres of radius $a_T = 100$ nm in xanthan solutions with a molecular weight of 2.2×10^6 g/mol.

IV. DISCUSSION

A. Diffusion time scales

There is no single consistent theory that treats tracer diffusion and sedimentation in polymer solutions for an arbitrary polymer concentration or tracer particle size. There are, however, a number of transport theories treating the limit of a strongly entangled network of immobilized polymers. At short times tracer diffusion in entangled polymer networks is retarded by hydrodynamic interactions (see Sec. IV B), while at intermediate and long times diffusion is additionally impeded by steric hindrance (obstruction effects) [8,10,61,66]. The appropriate theory with which to compare measured diffusion coefficients depends on the experimental time scales t_{expt}^r and t_{expt}^t on which tracer diffusion is measured, and on the characteristic time τ_{max} for relaxation of the transient meshes of the semidilute host polymer solution.

The experimental time scale for measuring tracer rotation, t_{expt}^r, with DDLS is independent of scattering angle and equal to $t_{\text{expt}}^r \cong 1/D_s^r$. In contrast, the experimental time scale for tracer translation, $t_{\text{expt}}^t = 1/D_s^t k^2$, is length scale dependent and set by the inverse wave vector, which in this work varied between $k_{\text{min}}^{-1} = 35$ and $k_{\text{max}}^{-1} = 120$ nm. In the limit of a rapidly fluctuating polymer solution with small τ_{max}, one will generally measure long-time tracer diffusion, unless the experimental time scales are very small. In the opposite limit of a cross-linked polymer network with $\tau_{\text{max}} \to \infty$ one will always measure the short-time rotational diffusion coefficient, D_s^r, since the neighborhood of the tracer is unchanging. Translational diffusion is, however, still frequency dependent. At short times one measures D_s^t, which is only affected by hydrodynamic interactions, while at long times one measures D_L^t, which is influenced by the tortuosity of the network and vanishes when the tracer is trapped.

We propose that a good choice for the typical polymer relaxation time τ_{max} is the experimentally observable crossover time $\tau_c = 1/\omega_c$, where $G' = G''$ [see Fig. 3(B)]. This time is a model-independent measure of the lifetime of the transient entanglements. At times t_{expt}^r, $t_{\text{expt}}^t \ll \tau_c$ the tracers perform rotational or translational diffusion in a predominantly elastic polymer network, while at times t_{expt}^r, $t_{\text{expt}}^t \gg \tau_c$ all polymer modes have decayed and the tracers sample a viscous environment. In Fig. 6(A) we compare the experimental times t_{exp}^r for rotation and $t_{\text{expt,min}}^t = k_{\text{min}}^{-2}/D_s^t$ and $t_{\text{expt,max}}^t = k_{\text{max}}^{-2}/D_s^t$ for translation with the crossover time τ_c. As seen, τ_c is always larger than t_{expt}^r and t_{expt}^t. We conclude that the measured diffusion coefficients are short-time quantities (D_s^r, D_s^t), affected by hydrodynamic interactions with the polymer network only. Accordingly, the experimental data are compared with hydrodynamic theories for tracer particle transport in semidilute polymer solutions, in Sec. IV C.

B. Hydrodynamic interactions in semidilute polymer solutions

While the static properties of semidilute solutions of (flexible) polymers in good solvents are fairly well understood [50], a consistent theoretical description of the dynamic properties of semidilute polymer solutions is lacking. In particular there is no general agreement regarding the range of the hydrodynamic interactions (HIs) and the importance of entanglements.

In dilute polymer solutions, HIs are described by the Oseen tensor [67] $\overleftrightarrow{T}_0$, whose trace decays as one over the
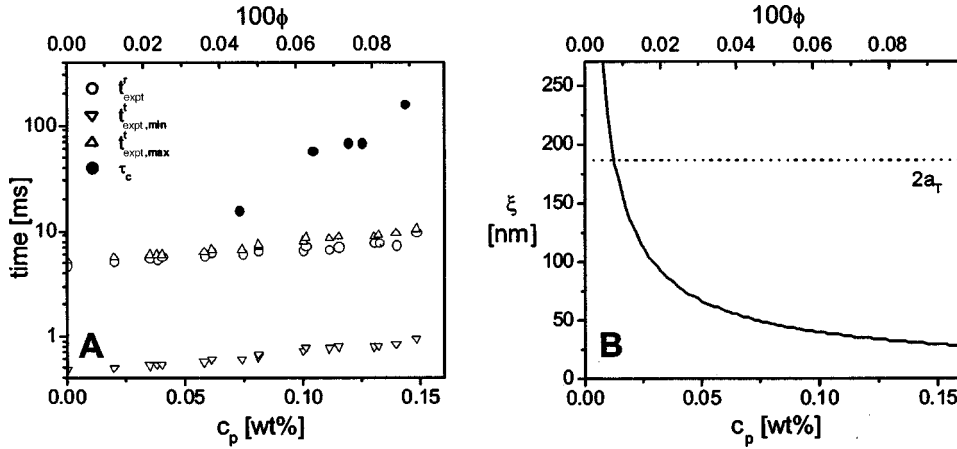
FIG. 6. Comparison between typical length and time scales of the host polymer solution and the tracer particle. (A) Concentration dependence of the tracer rotation time $\tau_{expt}^r = 1/D_s^r$ and translation times $t_{expt,min}^t = k_{min}^{-2}/D_s^t$ and $t_{expt,max}^t = k_{max}^{-2}/D_s^t$, compared with the crossover time τ_c of the xanthan solutions. (B) Concentration dependence of the static correlation length ξ of semidilute xanthan solutions, compared with the tracer sphere diameter $2a_T = 186$ nm.

distance r between two polymer segments. It has been conjectured that HIs between segments of a polymer chain in semidilute polymer solutions are screened to a short range by intervening polymer chains [68–75]. It is usually assumed that HIs are screened out completely at distances greater than the hydrodynamic screening length ξ_H. Screened HIs between two chain segments are then described by an exponential decay, $\vec{\vec{T}} = \vec{\vec{T}}_0 \exp(-r/\xi_H)$. Screening of HIs is known to occur for Darcy flow through a porous medium, which is composed of fixed frictional obstacles [76]. The conceptual difficulty with hydrodynamic screening in semidilute polymer solutions for some authors seems to be that the frictional obstacles are not fixed. It is therefore sometimes argued that hydrodynamic screening in polymer solutions is absent [77–81] or incomplete [82,83]. Freed and Perico [84] showed that in solutions of phantom polymer chains hydrodynamic screening is indeed absent because these freely intersecting chains are free to instantaneously follow the (perturbed) fluid flow. They proposed, however, that topological interactions (entanglements) between chains, which prevent them from passing through each other, impede the ability of the chains to drift freely with the solvent and therefore produce hydrodynamic screening. De Gennes [70] showed that modeling a semidilute polymer solution as an elastic temporary gel in a solvent leads to hydrodynamic screening.

The concentration dependence of the hydrodynamic screening length has also been a subject of considerable discussion [69–72,75]. According to the phenomenological theory of de Gennes [70] for flexible polymers in a good solvent, ξ_H is identical to the static correlation length ξ to within a numerical factor. The static correlation length represents the range of the monomer-monomer correlation function, i.e. the screening length of the excluded volume interactions between polymer segments [50]. On length scales below ξ, excluded volume interactions swell the chains so the chains are self-avoiding walks. On length scales greater than ξ, excluded volume interactions are screened, so the overall chain on this scale can be thought of as a random walk of blobs or renormalized monomers of radius ξ. The correlation length can also be thought of as the mesh size of the transient polymer network, being proportional to the mean distance between entanglement points [50]. The correlation length decreases with polymer concentration, since the

presence of other chains decreases the range of the monomer pair correlations:

$$\xi = R_g (c_p/c_p^*)^{-\beta}, \tag{9}$$

with exponent $\beta = 0.75$ in a good solvent and $\beta = 0.5$ in a theta solvent [50]. Experimentally, $\xi(c_p)$ for xanthan in $0.1M$ aqueous NaCl was shown [85] to follow Eq. (9) with $\beta = 0.75$. As shown in Fig. 6(B), the mesh size of the xanthan solutions decreases from 264 nm at $c_p^* = 0.008$ wt % to 28 nm at $c_p = 0.15$ wt % .

According to the theory of de Gennes [70], the screening length for excluded volume interactions is identical (apart from an unknown constant prefactor) to the hydrodynamic screening length, $\xi_H \cong \xi$. This prediction is supported by computer simulations [86] and experimental data [82,87,88], which suggest that $\xi_H/\xi \approx 1$. Our experimental data likewise support that $\xi_H/\xi \approx 1$, as demonstrated in Sec. IV C. Ahlrichs *et al.* [86] proposed that the latter identity arises because the obstacles that produce the Darcy-type frictional resistance are the blobs, i.e., chain portions between successive entanglement points. After the time needed for a blob to move its own size ξ, a polymer chain will, on average, feel the constraints of the temporary polymer network and is unable to follow the flow.

C. Hydrodynamic hindrance of tracer diffusion in semidilute polymer solutions

Hydrodynamic models for tracer particle transport in semidilute polymer solutions generally assume a hydrodynamic screening of the flow induced by the diffusing tracer [89–92]. A notable exception is the heuristic scaling theory of Phillies and co-workers [78–81], who argued that hydrodynamic screening in polymer solutions is absent and polymer entanglements are unimportant.

Phillies and co-workers derived scaling theories for self-translational [78–81] and rotational [79] diffusion of flexible linear polymer chains in dilute and semidilute solutions. A stretched exponential c_p dependence of the polymer self-diffusion coefficients of the form of Eq. (7) was derived by an extrapolation of dilute solution HI, obtained by the method of reflections, to larger concentrations using a self-

similarity assumption [78–80] or renormalization group theory [81]. The scaling prefactor α in Eq. (7) was found to depend on the strength of the HI, while the scaling exponent ν was found to range between 0.5 and 1 depending on the polymer molecular weight and the solvent quality, which control the extent of chain contraction. Based on experimental evidence that polymer self-diffusion and tracer sphere diffusion in polymer solutions are described by the same stretched exponential expression [58,93], Phillies and co-workers proposed that the same physical mechanism applies whatever the architecture of the tracer (flexible chain or rigid sphere). This statement is, however, disproved by recent experimental results for tracers of varying architecture immersed in the same matrix [60]. The rheological data reported in Sec. III A indicate that in our experimental system entanglements are important, so we do expect hydrodynamic screening to be present. Accordingly, we will compare our data with effective medium predictions for tracer diffusion assuming screened HIs.

Effective medium theories treat the polymer solution as a homogeneous Brinkman fluid with hydrodynamic screening length ξ_H. Altenberger and Tirrell [89,90] and Cukier [91] represented the polymers as points of hydrodynamic resistance and predicted stretched exponential c_p dependencies of the form $H_s^t \propto \exp(-A/\xi_H)$, where $\xi_H \propto c_p^{-\nu}$ is the hydrodynamic screening length. The exponent ν can take values between 0.5 and 0.75 depending on the chain stiffness and the solvent quality. The exponential prefactor A was not specified. Phillips [92] and Solomentsev and Anderson [13] used a somewhat different approach to calculate the hydrodynamic resistance of a homogeneous Brinkman medium with a hydraulic (or Darcy) permeability $k = \xi_H^2$. The permeability measures the resistance of the polymer network to a fluid flow. HIs of the tracer with the polymer solution were calculated from the phenomenological Brinkman equation [76], combining Darcy's law with the creeping flow equations

$$\eta \nabla^2 \vec{u} - \vec{\nabla} p - \frac{\eta}{k} \vec{u} = \vec{0}, \tag{10}$$

$$\vec{\nabla} \cdot \vec{u} = 0, \tag{11}$$

where $\vec{u}$ is the average fluid velocity and p is the pressure. Equations (10) and (11) were solved for the velocity field $\vec{u}$, assuming stick boundary conditions for the fluid velocity on the tracer surface. The stress tensor was then calculated from $\vec{u}$ and the force on the tracer was obtained by integrating the stress over the tracer surface. The reduced short-time translational diffusion coefficient was shown [13] to equal

$$H_s^t = \left[1 + \frac{a_T}{\sqrt{k}} + \frac{1}{9}\left(\frac{a_T}{\sqrt{k}} \right)^2 \right]^{-1}. \tag{12}$$

If the polymer solution indeed acts as a homogeneous Brinkman fluid, the translational drag experienced by a sedimenting tracer is expected to be equal to that experienced by a diffusing tracer, so s/s_0 should likewise follow Eq. (12). The
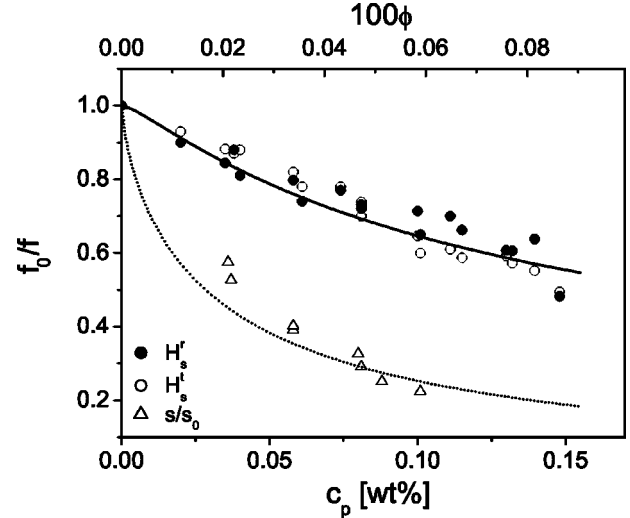

FIG. 7. Comparison of experimental data for reduced tracer rotational (H_s^r) and translational (H_s^t) diffusion and sedimentation (s/s_0) coefficients of PFA tracer spheres in xanthan solutions with theoretical predictions for translational (dotted line) and rotational (solid line) diffusion in a Brinkman medium [13].

rotational diffusion coefficient of a tracer in a Brinkman fluid was calculated in the same manner by Solomentsev and Anderson [13], who obtained

$$H_s^r = \frac{1 + a_T/\sqrt{k}}{1 + a_T/\sqrt{k} + 1/3(a_T/\sqrt{k})^2}. \tag{13}$$

A comparison of Eqs. (12) and (13) reveals that the retardation of tracer rotation is substantially less than the retardation of tracer translation for any value of $a_T/\sqrt{k}$ (or a_T/ξ_H).

In Fig. 7 the effective medium predictions according to Eqs. (12) and (13), taking $\xi_H = \xi$, are compared with the sedimentation and rotational and translational diffusion coefficients of the PFA tracers in the xanthan solutions. The reduced sedimentation coefficient s/s_0 is in excellent agreement with Eq. (12), while translational diffusion is much less retarded than predicted by Eq. (12). Unlike the translational diffusion coefficient, the rotational diffusion coefficient is in excellent agreement with the effective medium model [Eq. (13)].

The effective medium theory assumes that the tracer experiences a homogenous polymer solution. In reality the polymer segment density surrounding a tracer in a solution of nonadsorbing polymers is depleted over a certain distance. In dilute polymer solutions the typical thickness Δ of this depletion zone is approximately equal to the polymer radius of gyration R_g, while in semidilute solutions $\Delta \cong \xi$. When Δ is non-negligible compared to the tracer particle radius a_T, the tracer samples an inhomogeneous environment. In case of the xanthan-PFA mixtures the depletion zone thickness is appreciable compared to the tracer particle radius a_T, as seen in Fig. 6(B). This likely explains why translational tracer diffusion is less hindered than predicted by the effective medium theory. Apparently, tracer sedimentation is rela-
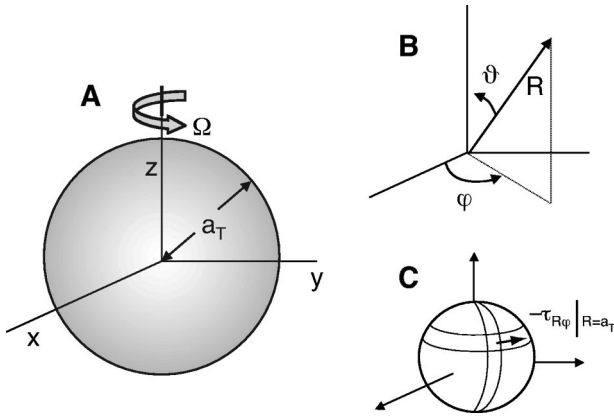
FIG. 8. (A) Colloidal tracer sphere with radius a_T placed in the origin, slowly rotating with an angular velocity Ω. (B) Spherical coordinates, with $0 \leq \varphi \leq 2\pi$ the azimuthal angle from the x axis in the xy plane, $0 \leq \vartheta \leq \pi$ the polar angle from the z axis, and R the distance from a point to the origin. (C) The tangential shear stress $\tau_{R\varphi}|_{R=a_T}$ exerted by a surface element $(a_T d\vartheta)(a_T \sin \vartheta d\varphi)$ on the fluid in the φ direction.

tively insensitive to the local depletion-induced inhomogeneities. This can be traced to the different experimental time and length scales of a diffusion experiment and a sedimentation measurement. Translational diffusion is measured on time scales of 10^{-3} s and length scales of 10^{-7} m, while sedimentation is monitored on macroscopic length scales of 10^{-2} m and time scales of hours to days. The time required for a tracer to sediment over a distance ξ is much longer (about 11 s) than the lifetime of the meshes (10–100 ms), while the time required for a tracer to diffuse a distance ξ is much shorter (~ 1 ms). It is therefore plausible that a sedimenting tracer experiences a homogeneous medium while a diffusing tracer does not.

The good agreement of the rotational tracer diffusion coefficients H_s^r with the effective medium theory does not necessarily imply that a rotating tracer experiences a homogeneous Brinkman medium. We will clarify this statement by considering a simple model of a tracer particle rotating in a concentric spherical confinement that represents a depletion cavity. This model at the same time mimics the basic idea of hydrodynamic screening and accounts for a locally inhomogeneous polymer solution.

The rotational diffusion coefficient is calculated here by solving the Stokes equations for a tracer particle rotating in pure solvent contained in a concentric spherical depletion cavity of radius ξ. The polymers are assumed to be completely depleted from this cavity. This is of course a simplification of the actual polymer segment concentration profile, which rises smoothly from zero at the particle surface to the bulk density far from the surface. The depletion cavity has a volume $V_c = (4/3)\pi a_T^3 (1+\delta)^3$, where $\delta a_T = \Delta$ is the thickness of the depleted zone ($0 \leq \delta$). The velocity distribution $\vec{u}$ induced in the fluid by a sphere rotating about the z-axis clearly has to be symmetrical about the z axis, with the fluid moving in annuli about the axis of symmetry [Fig. 8(A)]. In spherical coordinates φ, ϑ, and R [Fig. 8(B)] this implies that the fluid velocity components u_ϑ and u_R are zero, while u_φ

$= u_\varphi(\vartheta, R)$. The boundary conditions on u_φ for a sphere rotating with a constant angular velocity Ω in an unbounded pure fluid ($\delta \to \infty$) are [22]

$$u_\varphi = 0, \quad r \to \infty, \tag{14a}$$

$$u_\varphi = a_T \Omega \sin \vartheta, \quad r \to a_T, \tag{14b}$$

where r is the radial distance from the sphere surface. Due to hydrodynamic screening by the polymers the velocity field must decay to zero at a finite value of r. For this finite value we simply choose $a_T(1+\delta)$, which is the position of the surface of the depletion cavity. Stick boundary conditions on the sphere surface and on the polymers imply

$$u_\varphi = 0, \quad r \to a_T(1+\delta), \tag{15a}$$

$$u_\varphi = a_T \Omega \sin \vartheta, \quad r \to a_T. \tag{15b}$$

The velocity field $u_\varphi = C_1 r + (C_2/r^2)\sin \vartheta$ satisfying these boundary conditions is

$$u_\varphi = \Omega a_T \sin \vartheta \left(\frac{r}{a_T}\right)\left[\frac{1}{1-(1+\delta)^3}\right] + \Omega a_T \sin \vartheta \left(\frac{a_T}{r}\right)^2 \left[\frac{(1+\delta)^3}{(1+\delta)^3 - 1}\right], \tag{16}$$

which can be substituted in Newton's viscosity law [67] for the tangential stress $\tau_{r\varphi}$ [see Fig. 8(C)]:

$$\tau_{r\varphi} = -\eta_0 r \frac{\partial}{\partial r}\left(\frac{u_\varphi}{r}\right). \tag{17}$$

Integration of Eq. (17) over the sphere surface yields the total torque T_z on the sphere:

$$T_z = 8\pi\eta_0 a_T^3 \frac{(1+\delta)^3}{(1+\delta)^3 - 1}\Omega. \tag{18}$$

The expression multiplying the angular velocity Ω is the friction factor f_s^r. The rotational diffusion coefficient $D_s^r = k_B T/f_s^r$ of the sphere centered in the depletion cavity is therefore

$$D_s^r = \frac{k_B T}{8\pi\eta_0 a_T^3}\left[\frac{(1+\delta)^3}{(1+\delta)^3 - 1}\right]^{-1}, \quad \delta = \Delta/a_T. \tag{19}$$

For a very large cavity ($\delta \gg 1$), Eq. (19) reduces to the familiar Stokes-Einstein-Debye result $D_s^r = D_0^r = k_B T/(8\pi\eta_0 a_T^3)$. For semidilute solutions the depletion layer thickness Δ equals the static correlation length ξ, so the reduced rotational diffusion coefficient is

$$H_s^r = \frac{(1 + \xi/a_T)^3 - 1}{(1 + \xi/a_T)^3}. \tag{20}$$

As shown in Fig. 9, Eq. (20) is almost indistinguishable from the effective medium prediction Eq. (13), and in good agreement with the experimental data.
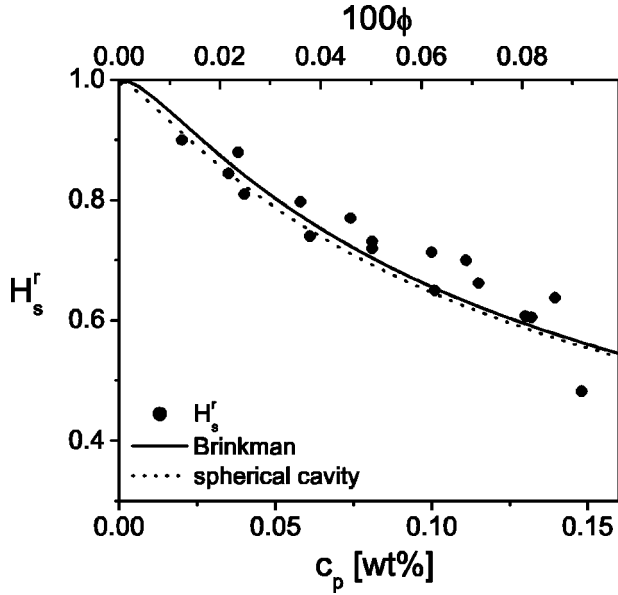
FIG. 9. Comparison of the reduced rotational diffusion coefficient H_s^r of PFA tracer spheres in xanthan solutions with the theoretical prediction for a Brinkman medium [13] and for a sphere in a concentric spherical cavity with a radius equal to the hydrodynamic screening length ξ_H.

The assumptions underlying Eq. (20) are reasonable because a rotating spherical tracer does not displace fluid and therefore samples only its local environment when HIs are screened from a finite distance away from the sphere. In this respect Eq. (20) comprises the basic idea of hydrodynamic screening. At the same time, it accounts for the rotational diffusion of a tracer particle in a locally inhomogeneous polymer solution due to depletion. Since Eqs. (13) and (20) produce the same hindrance they do not justify a clear conclusion about the extent to which a rotating sphere experiences a homogeneous Brinkman fluid.

In contrast to a rotating sphere, a translating sphere does displace fluid, leading to solvent backflow outside the cavity. We also note here that modelling the cavity by an impermeable outer sphere produces a translational friction for the off-center motion of the inner sphere which is much larger [67] than observed in our experiments. Consequently a "local model" of a translating particle in a spherical depletion cavity, analogous to Eq. (20), does not apply. Hence, it is not clear how the effective medium theories should be modified to take into account the polymer depletion layer. For small tracers ($a_T \ll \xi$) in semidilute solutions of flexible polymers ($a_T \gg 2q$)—where collective diffusion of the polymer meshes is much slower than the tracer diffusion time—Odijk [9] derived a depletion transport theory that takes into account the dynamics of the reorganization of the depletion zone as the particle diffuses ("dynamic depletion"). This model is, however, not applicable to the PFA-xanthan solutions, since the tracers are large compared to the polymer meshes [cf. Fig. 6(B)] and the polymers are semiflexible (a_T is close to q).

D. Stokes-Einstein scaling

Figure 5 shows that the macroscopic low-shear viscosity η_L of the polymer solutions severely overestimates the retardation of tracer diffusion and sedimentation. Deviations from the generalized Stokes relation [Eq. (8)], usually referred to as deviations from "Stokes-Einstein behavior," are generally rationalized in terms of a scaling approach proposed by Langevin and Rondelez [62]. This approach employs static arguments, identifying a_T/ξ as the key parameter. For tracer sizes $a_T \ll \xi$ the tracer is supposed to be largely unaffected by the polymer, probing a local viscosity close to the solvent viscosity η_0. Tracers with sizes $a_T \gg \xi$, on the other hand, are supposed to probe the macroscopic viscosity η_L. The two limits are bridged by a scaling function of a_T/ξ, dependent only on the polymer concentration c_p. In line with these scaling arguments, the drag on large tracer particles [3,5,24,64,65] in semidilute (and dilute) polymer solutions often agrees with the generalized Stokes law, while small tracers [1,2,4,6,60] experience a smaller friction. Since the radius a_T of the PFA tracers is larger than the average mesh size ξ of the xanthan solutions for xanthan concentrations $c_p > 0.02$ wt % [Fig. 6(B)], the Langevin-Rondelez scaling approach would lead one to expect that the generalized Stokes relation should work quite well. However, the scaling approach completely disregards the dynamics of the polymer solution. As discussed in Sec. IV A, the lifetime of the polymer entanglements is longer than the diffusion times of the tracer particles. The tracers therefore experience a predominantly elastic polymer solution. Rather than comparing the short-time diffusion coefficients D_s^r and D_s^t with the low-shear viscosity, one should compare them with the "short-time," high-frequency-limiting viscosity η_∞:

$$1/H_s^r = 1/H_s^t = \eta_0/\eta_\infty. \quad (21)$$

This short-time Stokes-Einstein relation, like Eq. (8), still assumes that the tracer sees a continuous environment. The issue of the frequency dependence of the friction factor for a tracer in a semidilute polymer solution has hitherto not been explicitly considered in the literature on tracer diffusion in polymer solutions.

For the entangled xanthan solutions the high-frequency-limiting viscosity η_∞ was experimentally inaccessible since inertia effects permit a maximum frequency in our set-up of only 67 rad/s. As shown in Fig. 5, the inverse reduced dynamic viscosity η_0/η_{67}' measured at 67 rad/s still overestimates the friction experienced by the tracer particles. To measure the high-frequency-limiting viscosity of the xanthan solutions one could resort to torsional resonator rheometers [94] or micorheology techniques [95].

The generalized Stokes relations assume that on the length scale a_T of the tracer particle, the polymer solution can be considered homogeneous. This ignores the depletion of polymer segments over a distance $\Delta \cong \xi$ around the tracer [9,60]. When Δ is non-negligible compared to a_T, the tracer samples an inhomogeneous environment with a viscosity that rises from the solvent viscosity η_0 at its surface, where $c_p = 0$, to the bulk viscosity η_L at large distances from the

surface. This will reduce the effective viscosity experienced by the tracer relative to the generalized Stokes prediction. For large tracers ($a_T > R_g$) in dilute nonadsorbing polymer solutions one can correct for this effect since the depletion layer reorganizes fast, so the polymer segment concentration profile near the tracer is to a good approximation equal to the equilibrium distribution [96–98]. The xanthan-colloid mixtures are not in this limit, so no quantitative predictions of the depletion effect are available. However, since Δ is 0.3–3 times a_T, depletion effects are certainly expected to reduce the friction coefficient relative to the continuum generalized Stokes prediction. The effect is expected to be enhanced with larger Δ/a_T and a larger bulk solution viscosity.

V. CONCLUSIONS

We presented experimental data for rotational and translational diffusion as well as sedimentation of tracer spheres in semidilute solutions of the semiflexible, nonadsorbing polymer xanthan. The rotational and translational diffusion coefficients of the tracer spheres have virtually the same dependence on the xanthan concentration, while tracer sedimentation is substantially more hindered in the xanthan solutions.

Steady and oscillatory shear data indicate that the xanthan solutions behave dynamically like model semidilute polymeric solutions with fairly long-lived topological entanglements for concentrations c_p above the overlap concentration of $c_p^* = 0.008$ wt %. The scaling of the viscosity and linear viscoelastic moduli with frequency, shear rate and polymer concentration is in agreement with theoretical predictions for entangled polymers.

On the time scale of tracer motion the xanthan solutions in the concentration regime studied ($c_p/c_p^* = 1-18$) are predominantly elastic. The generalized SE relation describing the polymer solution as a continuous viscous fluid therefore overestimates the tracer hindrance by two orders of magnitude. Instead, effective medium theory, describing the polymer solution as a homogeneous Brinkman fluid with a hydrodynamic screening length equal to the concentration dependent static correlation length ξ, is in excellent agreement with the measured sedimentation and rotational diffusion coefficients. Rotational diffusion, however, is at the same time well quantified by a simple model of a rotating sphere in a concentric spherical depletion cavity. This model comprises the basic idea of hydrodynamic screening but also accounts for a locally inhomogeneous polymer solution due to depletion. It is therefore unclear to what extent a rotating tracer sphere experiences a homogeneous Brinkman fluid. Translational diffusion is faster than predicted by the effective medium theory, likely due to the locally inhomogeneous environment of the tracers arising from segment depletion. Our results clearly show the need for a theory that combines depletion effects, hydrodynamic interactions, and, for intermediate and long times, obstruction effects.

[1] T.-H. Lin and G. D. J. Phillies, Macromolecules **17**, 1686 (1984).

[2] T. Yang and A. M. Jamieson, J. Colloid Interface Sci. **126**, 220 (1988).

[3] Z. Pu and W. Brown, Macromolecules **22**, 890 (1989).

[4] R. Furukawa, J. L. Arauz-Lara, and B. R. Ware, Macromolecules **24**, 599 (1991).

[5] C. N. Onyenemezu, D. Gold, M. Roman, and W. G. Miller, Macromolecules **26**, 3833 (1993).

[6] M. A. Tracey, J. L. Garcia, and R. Pecora, Macromolecules **26**, 1862 (1993).

[7] D. Gold, C. Onyenemezu, and W. G. Miller, Macromolecules **29**, 5700 (1996).

[8] L. Masaro and X. X. Zhu, Prog. Polym. Sci. **24**, 731 (1999).

[9] T. Odijk, Biophys. J. **79**, 2314 (2000).

[10] B. Amsden, Polymer **43**, 1623 (2002).

[11] D. Sohn, P. S. Russo, A. Davila, D. S. Poche, and M. L. McLaughlin, J. Colloid Interface Sci. **177**, 31 (1996).

[12] D. S. Clague and R. J. Phillips, Phys. Fluids **8**, 1720 (1996).

[13] Y. E. Solomentsev and J. L. Anderson, Phys. Fluids **8**, 1119 (1996).

[14] B. Camins and P. S. Russo, Langmuir **10**, 4053 (1994).

[15] T. Jamil and P. S. Russo, Langmuir **14**, 264 (1998).

[16] B. Katzbauer, Polym. Degrad. Stab. **59**, 81 (1998).

[17] P. J. Whitcomb, J. Rheol. **22**, 493 (1978).

[18] Y. Takada, T. Sato, and A. Teramoto, Macromolecules **24**, 6215 (1991).

[19] H.-C. Lee and D. A. Brant, Macromolecules **35**, 2223 (2002).

[20] H.-C. Lee and D. A. Brant, Macromolecules **35**, 2212 (2002).

[21] G. H. Koenderink, D. G. A. L. Aarts, V. W. A. De Villeneuve, A. P. Philipse, R. Tuinier, H. N. W. Lekkerkerker, Biomacromolecules **4**, 129 (2003).

[22] G. G. Stokes, Proc. Cambridge Philos. Soc. **9**, 8 (1851).

[23] N. Nemoto, T. Inoue, Y. Makita, Y. Tsunashima, and M. Kurata, Macromolecules **18**, 2516 (1985).

[24] O. A. Nehme, V. Johnson, and A. M. Donald, Macromolecules **22**, 4326 (1989).

[25] X. Ye, P. Tong, and L. J. Fetters, Macromolecules **31**, 5785 (1998).

[26] I. Capron, G. Brigand, and G. Muller, Polymer **38**, 5289 (1997).

[27] I. Capron, S. Alexandre, and G. Muller, Polymer **39**, 5725 (1998).

[28] T. Coviello, K. Kajiwara, W. Burchard, M. Dentini, and V.

Crescenzi, Macromolecules **19**, 2826 (1986).

[29] A. B. Rodd, D. E. Dunstan, and D. V. Boger, Carbohydr. Polym. **42**, 159 (2000).

[30] S. Paoletti, A. Cesàro, and F. Delben, Carbohydr. Res. **123**, 173 (1983).

[31] T. Sato, T. Norisuye, and H. Fujita, Macromolecules **17**, 2696 (1984).

[32] H.-C. Lee and D. A. Brant, Biomacromolecules **3**, 742 (2002).

[33] H. W. Oviatt, Jr. and D. A. Brant, Macromolecules **27**, 2402 (1994).

[34] G. Berth, H. Dautzenberg, B. E. Christensen, S. E. Harding, G. Rother, and O. Smidsrod, Macromolecules **29**, 3491 (1996).

[35] M. Milas, W. F. Reed, and S. Printz, Int. J. Biol. Macromol. **18**, 211 (1996).

[36] A. Gamini and M. Mandel, Biopolymers **34**, 783 (1994).

[37] H. Benoit and P. Doty, J. Phys. Chem. **57**, 958 (1953).

[38] B. Tinland, G. Maret, and M. Rinaudo, Macromolecules **23**, 596 (1990).

[39] G. Chauveteau, J. Rheol. **26**, 111 (1982).

[40] R. K. Richardson and S. B. Ross-Murphy, Int. J. Biol. Macromol. **9**, 257 (1987).

[41] R. Piazza, Phys. Scr. **T49**, 94 (1993).

[42] V. Degiorgio, R. Piazza, and T. Bellini, Adv. Colloid Interface Sci. **48**, 61 (1994).

[43] R. J. Hunter, *Zeta Potential in Colloid Science* (Academic Press, London, 1981).

[44] V. Degiorgio, R. Piazza, and T. Bellini, in *Observation, Prediction and Simulation of Phase Transitions in Complex Fluids*, edited by M. Baus *et al.* (Kluwer, Dordrecht 1995).

[45] T. Biben and J.-P. Hansen, J. Phys.: Condens. Matter **6**, A345 (1994).

[46] R. Van Roij, J. Phys.: Condens. Matter **15**, 53569 (2003).

[47] M. L. Huggins, J. Am. Chem. Soc. **64**, 2716 (1942).

[48] I. Capron, G. Brigand, and G. Muller, Int. J. Biol. Macromol. **23**, 215 (1998).

[49] M. Muthukumar and K. F. Freed, Macromolecules **10**, 899 (1977).

[50] P.-G. De Gennes, *Scaling Concepts in Polymer Physics* (Cornell University Press, Ithaca, NY, 1979).

[51] M. Doi and S. F. Edwards, *The Theory of Polymer Dynamics* (Clarendon, Oxford, 1988).

[52] W. W. Graessley, Adv. Polym. Sci. **16**, 1 (1974).

[53] A. M. Jamieson, J. G. Southwick, and J. Blackwell, J. Polym. Sci., Polym. Phys. Ed. **20**, 1513 (1982).

[54] M. Milas, M. Rinaudo, M. Knipper, and J. L. Schuppiser, Macromolecules **23**, 2506 (1990).

[55] J. D. Ferry, *Viscoelastic Properties of Polymers* (Wiley, New York, 1980).

[56] W. P. Cox and E. H. Merz, J. Polym. Sci. **28**, 619 (1958).

[57] J. O. Carnali, J. Appl. Polym. Sci. **43**, 929 (1991).

[58] G. D. J. Phillies, Macromolecules **19**, 2367 (1986).

[59] J. Won, C. Onyenemezu, W. G. Miller, and T. P. Lodge, Macromolecules **1994**, 7389 (1994).

[60] Y. Cheng, R. K. Prud'homme, and J. L. Thomas, Macromolecules **35**, 8111 (2002).

[61] A. G. Ogston, B. N. Preston, and J. D. Wells, Proc. R. Soc. London, Ser. A **333**, 297 (1973).

[62] D. Langevin and F. Rondelez, Polymer **19**, 875 (1978).

[63] P. Tong, X. Ye, B. J. Ackerson, and L. J. Fetters, Phys. Rev. Lett. **79**, 2363 (1997).

[64] W. Brown and R. Rymden, Macromolecules **21**, 840 (1988).

[65] S. G. J. M. Kluijtmans, G. H. Koenderink, and A. P. Philipse, Phys. Rev. E **61**, 626 (2000).

[66] L. Johansson, C. Elvingson, and J.-E. Lofroth, Macromolecules **24**, 6024 (1991).

[67] J. Happel and H. Brenner, *Low Reynolds Number Hydrodynamics* (Noordhoff, Leiden, 1973).

[68] S. F. Edwards and K. F. Freed, J. Chem. Phys. **61**, 1189 (1974).

[69] K. F. Freed and S. F. Edwards, J. Chem. Phys. **61**, 3626 (1974).

[70] P.-G. De Gennes, Macromolecules **9**, 594 (1976).

[71] M. Muthukumar and S. F. Edwards, Polymer **23**, 345 (1982).

[72] S. F. Edwards and M. Muthukumar, Macromolecules **17**, 586 (1984).

[73] M. Muthukumar, Macromolecules **21**, 2891 (1988).

[74] Y. Shiwa, Y. Oono, and P. R. Baldwin, Macromolecules **21**, 208 (1988).

[75] G. H. Fredrickson and E. Helfand, J. Chem. Phys. **93**, 2048 (1990).

[76] H. C. Brinkman, Appl. Sci. Res., Sect. A **1**, 27 (1947).

[77] Y. Oono and P. R. Baldwin, Phys. Rev. Lett. **53**, 2149–2152 (1984).

[78] G. D. J. Phillies, Macromolecules **20**, 558 (1987).

[79] G. D. J. Phillies, Macromolecules **21**, 3101 (1988).

[80] G. D. J. Phillies, J. Phys. Chem. **93**, 5029 (1989).

[81] G. D. J. Phillies, Macromolecules **31**, 2317 (1998).

[82] D. Richter, K. Binder, B. Ewen, and B. Stühn, J. Phys. Chem. **88**, 6618 (1984).

[83] J. E. Martin, Macromolecules **19**, 1278 (1986).

[84] K. F. Freed and A. Perico, Macromolecules **14**, 1290 (1981).

[85] D. Auserre, M. Hervet, and F. Rondelez, Phys. Rev. Lett. **54**, 1948 (1985).

[86] P. Ahlrichs, R. Everears, and B. Duenweg, Phys. Rev. E **64**, 040501 (2001).

[87] P. Wiltzius, H. R. Haller, D. S. Cannell, and D. W. Schaefer, Phys. Rev. Lett. **53**, 834 (1984).

[88] K. J. Zhang, M. E. Briggs, R. W. Gammon, J. V. Sengers, and J. F. Douglas, J. Chem. Phys. **111**, 2270 (1999).

[89] A. R. Altenberger and M. Tirrell, J. Polym. Sci., Polym. Phys. Ed. **22**, 909 (1984).

[90] A. R. Altenberger and M. Tirrell, J. Chem. Phys. **80**, 2208 (1984).

[91] R. I. Cukier, Macromolecules **17**, 252 (1984).

[92] R. J. Phillips, Biophys. J. **79**, 3350 (2000).

[93] G. D. J. Phillies, G. S. Ullmann, K. Ullmann, and T.-H. Lin, J. Chem. Phys. **82**, 5242 (1985).

[94] J. C. Van der Werff, C. G. De Kruif, C. Blom, and J. Mellema, Phys. Rev. A **39**, 795 (1989).

[95] F. C. MacKintosh and C. F. Schmidt, Curr. Opin. Colloid Interface Sci. **4**, 300 (1999).

[96] E. Donath, A. Krabi, M. Nirschl, V. M. Shilov, M. I. Zharkikh, and B. Vincent, J. Chem. Soc., Faraday Trans. **93**, 115 (1997).

[97] C. W. Hoogendam, J. C. W. Peters, R. Tuinier, A. de Keizer, M. A. Cohen-Stuart, and B. H. Bijsterbosch, J. Colloid Interface Sci. **207**, 309 (1998).

[98] A. J. Levine and T. C. Lubensky, Phys. Rev. E **63**, 041510 (2001).